Automatika

Journal for Control, Measurement, Electronics, Computing and Communications

ISSN: (Print) (Online) Journal homepage: https://www.tandfonline.com/loi/taut20

An asinh-type regulator for robot manipulators with global asymptotic stability

Fernando Reyes-Cortes & Basil M. Al-Hadithi

To cite this article: Fernando Reyes-Cortes & Basil M. Al-Hadithi (2020) An asinh-type regulator for robot manipulators with global asymptotic stability, Automatika, 61:4, 574-586, DOI: 10.1080/00051144.2020.1796111

To link to this article: https://doi.org/10.1080/00051144.2020.1796111

Published online: 28 Jul 2020.

AUTOMATIKA
2020, VOL. 61, NO. 4, 574–586
https://doi.org/10.1080/00051144.2020.1796111

REGULAR PAPER

OPEN ACCESS Check for updates

An asinh-type regulator for robot manipulators with global asymptotic stability

Fernando Reyes-Cortes [a] and Basil M. Al-Hadithi [b,c]

[a]Facultad de Ciencias de la Electrónica, Benemérita Universidad Autónoma de Puebla, Puebla, Mexico; [b]Centre for Automation and Robotics UPM - CSIC, Intelligent Control Group, Universidad Politecnica de Madrid, Madrid, Spain; [c]Department of Electrical, Electronics, Control Engineering and Applied Physics, Higher Technical School of Industrial Design and Engineering, Universidad Politecnica de Madrid, Madrid, Spain

ABSTRACT

In this paper, a new asinh-type control scheme with gravity compensation for the position control problem of robot manipulators in joint space is presented. The properties and characteristics of the asinh control structure make the position error and the motion velocity asymptotically converge to the equilibrium point. A strict Lyapunov function to formally prove global asymptotic stability is developed. The tuning of the control gains is obtained by PSO (Particle Swarm Optimization) technique without saturating the servomotors. To illustrate the effectiveness and performance of the proposed scheme, an experimental comparative analysis between the proportional-derivative (PD) and atanh controls against the proposed algorithm on a three degrees of freedom direct-drive robot manipulator is carried out.

ARTICLE HISTORY
Received 5 June 2019
Accepted 26 June 2020

KEYWORDS
Asinh control; robot manipulator; global asymptotic stability; position control; PSO algorithm

1. Introduction

Robot manipulators have several applications such as pick-and-place operations, paintings, circuit-board assembly, drilling, palletizing, physiotherapy, robotic operating rooms, etc. These applications are carried out correctly through high-performance position control algorithms [1]. The joint position control problem (also, so-called regulation) of robot manipulators consists in moving freely in its workspace the manipulator end-effector from any initial condition to a configuration of fixed desired position, which is assumed to be constant, regardless of its initial joint position [1,2].

The linear PD control is the simplest one to achieve regulation of robot manipulators. This control guarantees the global regulation objective [3]. However, the PD control keeps a non-zero error in steady state. In order to decrease this error, the proportional-integral-derivative (PID) control is proposed. But until now, the PID control lacks of global asymptotic stability. It is valid only in a local sense [2,4,5].

The position problem of robot manipulators is still a research area with challenging problems. It has become a permanent and systematic scientific activity to design new control schemes of high performance with several potential applications. In [5], a fuzzy control scheme with bounded torques is presented and the global asymptotic stability via Lyapunov theory is proven with an experimental evaluation. Studies on the stability properties of robot manipulators under the action of saturated PID control are reported in [6]. A global stable nonlinear PID with saturated functions is developed in [7]. Experimental results on a 2-degrees-of-freedom (dof) robot manipulator are presented. In [8], the global asymptotic regulation under input constrains is addressed. A saturated PID control in agreement with Lyapunov's direct method and LaSalle's invariance principle is presented. The proposed approach is illustrated via simulations.

In [9], a nonlinear PID control with bounded torque is presented. Global asymptotic stability is proven via Lyapunov stability theory, and experimental results are included. In [10] a saturated control of a general class of uncertain nonlinear systems with time-delayed actuation and additive bounded disturbances is analyzed. The performance of the controller is demonstrated via simulation on a two-dof planar robot manipulator. The authors in [11] propose the formulation of 2 PD schemes to control a flexible joint robot manipulators subject to actuator saturation, while simultaneously guaranteeing asymptotic stability about equilibrium point of the closed-loop system. Experimental results on a single-link flexible-joint manipulator are reported.

In [12], a saturated PID control of double integrator with bounded disturbance and sufficient conditions for stability is analyzed. The effectiveness of the proposed control scheme is validated via numerical simulations. A PID-type control with global position stabilization for bounded inputs is analyzed in [13]. Experimental tests on a two-dof robot manipulator are

CONTACT Fernando Reyes-Cortes fernando.reyes@correo.buap.mx

presented. In [14] a family of nonlinear PID-like controls is described. Lyapunov theory is used to establish conditions for local asymptotic stability. Experimental results complement the proposed schemes. The work in [15], addresses the problem of robust regulation and trajectory tracking via energy shaping to stabilize a control scheme with two terms; a partial linearizing state-feedback and a linear PID loop around two passive outputs. In this work, no experimental/ simulation results are included.

Recently, a nonlinear switching PD plus gravity compensation is analyzed with global asymptotic stability through Lyapunov's direct method [16]. Experimental results of the proposed control on a one-dof robotic system are presented. In [17], a torque to position conversion method for position commanded servomotors in robot manipulators is presented. The proposed conversion law is combined with a backstepping sliding mode control. The stability analysis is shown through Lyapunov's theory. However, the conditions to ensure stability are complex. They depend of structured uncertainty due to modeling error and system noise due to feedback. To validate the proposed method, experimental studies are tested on a 3-dof mechanical systems. A nonlinear PID control is proposed in [18]. Lyapunov stability is employed to prove global finite-time stability.

In [19], a flexible one-dof manipulator with input disturbances and output constraints is considered. With the Lyapunov's direct method, a boundary control with tanh structure is designed to regulate the joint position and suppress elastic vibration simultaneously. Numerical simulations are analyzed to demonstrate the effectiveness of the proposed scheme. In [20], the study of the PID control to regulate the position of a robot whit 4-dof by decoupling the dynamic model is presented. This work does not present stability analysis. Numerical simulations for a planar robot are carried out. The work [21] adopts a PID position regulation with proof of global asymptotic stability using LaSalle invariance principle taking into account the electric dynamics of the permanent magnet synchronous actuators of the robot. Experimental results on a two dof direct-drive robot are analyzed. In [22] the regulation problem for a one-dof Euler-Lagrange system with the motor electric dynamics is considered. The global stability analysis is carried out through a PID control using LaSalle invariance principle.

The work [23] deals with the problem of controlling a 7-dof Baxter robot, whose joints have bounded position, velocity, and acceleration/torque. The control schemes used are PD-Type. Stability analysis is not studied in this work. Simulation results are presented. In [24], the problem of robust tracking control of electrically flexible joint robots through a nonlinear PID-type proposed control scheme is addressed. Experimental results demonstrate high performance of the proposed control on a flexible-joint electrically driven robot. On the other hand, since the pioneering work of Takegaki and Arimoto in 1981 [3] on energy shaping methodology, which uses a special class of artificial potential energies for generating control schemes, the derivative control action is employed to obtain damping injection for avoiding overshoot reduction in the transient response. The method of energy shaping has been followed by several authors [25–28].

It is important to note that from previous works, not all of them present experimental results. There are still several papers with simulations only, which are important, but do not reflect the robustness and actual control performance in a real physical robot. In addition, we remark that few works develop asymptotic stability analysis using strict Lyapunov functions. Within this context, in this paper using energy shaping, we propose a asinh-type control scheme with gravity compensation for the global regulation problem of robot manipulators in joint space. The proposed algorithm has properties, qualities and a different mathematical structure to the previously cited works. The hyperbolic structure acts like a nonlinear spring that tries to restore the position error to zero, and the derivative action has a behavior similar to a nonlinear damper that dissipates the motion generated by the velocity. The above features are used to obtain transitory-state response without overshoots, good rising and settling time and also to asymptotically drive the position error to zero.

Therefore, the main contributions of this paper are to formally prove that the closed-loop system equilibrium point is globally asymptotically stable using a new structure of strict Lyapunov function avoiding to use the Krasovskii-LaSalle theorem (the proposed strict Lyapunov function has not been used in previous works). Moreover, an experimental comparison between the well known PD control and control algorithm with atanh structure against the proposed algorithm on a three dof direct-drive robot manipulator is presented. The tuning of the control gains is obtained by PSO technique guaranteeing that the demanded torques remain inside the prescribed limits in the servomotors. These arguments constitute the motivation for this work.

This paper is organized as follows. Section 2 describes the dynamics of rigid robots and its main properties. The main results of this work, i.e. the proposed asinh-type control and its global asymptotic stability proof of the closed-loop system equilibrium point are stated in the Section 3. Experimental results are shown in the Section 4. Section 5 presents future research to be handled. Finally, conclusions are given in Section 6.

2. Robot dynamics

The dynamics model for a serial n-link rigid robot with viscous friction and n dof can be written as [1,2]:

$$\boldsymbol{\tau} = M(\boldsymbol{q})\ddot{\boldsymbol{q}} + C(\boldsymbol{q},\dot{\boldsymbol{q}})\dot{\boldsymbol{q}} + \boldsymbol{g}(\boldsymbol{q}) + B\dot{\boldsymbol{q}} \qquad (1)$$

where $\boldsymbol{q}, \dot{\boldsymbol{q}}, \ddot{\boldsymbol{q}} \in \mathbb{R}^n$ are the joint vectors of position, velocity and acceleration, respectively; $\boldsymbol{\tau} \in \mathbb{R}^n$ is the vector of applied torques to the robot joints; $M(\boldsymbol{q}) \in \mathbb{R}^{n\times n}$ is the inertia matrix; $C(\boldsymbol{q},\dot{\boldsymbol{q}}) \in \mathbb{R}^{n\times n}$ represents the matrix of centripetal and Coriolis torques; $\boldsymbol{g}(\boldsymbol{q}) \in \mathbb{R}^n$ is the vector of gravitational torques, and $B \in \mathbb{R}^{n\times n}$ is the matrix for the viscous friction.

We assume that all the robot links are revolute-type joints. The equation of motion (1) has several fundamental properties to facilitate control scheme analysis [1,2].

Property 2.1: The inertia matrix $M(\boldsymbol{q}) \in \mathbb{R}^{n\times n}$ is symmetric and positive definite. It satisfies:

$$M(\boldsymbol{q}) = M^T(\boldsymbol{q}) \Longleftrightarrow M^{-1}(\boldsymbol{q}) = M^{-T}(\boldsymbol{q}), \quad \forall \boldsymbol{q} \in \mathbb{R}^n \qquad (2a)$$

$$M(\boldsymbol{q}) > 0 \Longleftrightarrow M^{-1}(\boldsymbol{q}) > 0, \quad \forall \boldsymbol{q} \in \mathbb{R}^n \qquad (2b)$$

$$\boldsymbol{x}^T M(\boldsymbol{q})\boldsymbol{x} > 0 \Longleftrightarrow \boldsymbol{x}^T M^{-1}(\boldsymbol{q})\boldsymbol{x} > 0, \quad \forall \boldsymbol{q}, \boldsymbol{x} \in \mathbb{R}^n \qquad (2c)$$

Property 2.2: For robots having only revolute joints, there exists a positive constant $\beta_M > 0$ such that, $\|M(\boldsymbol{q})\| \leq \lambda_M^{\max} < \beta_M$; where $\lambda_M^{\max}$ is the maximum eigenvalue of the inertia matrix $M(\boldsymbol{q})$.

Property 2.3: If $\dot{\boldsymbol{q}} = \boldsymbol{0}$, then the centrifugal and Coriolis torques matrix $C(\boldsymbol{q},\dot{\boldsymbol{q}})$ satisfies $C(\boldsymbol{q},\boldsymbol{0}) = 0 \in \mathbb{R}^{n\times n}\ \forall \boldsymbol{q} \in \mathbb{R}^n$.

Property 2.4: The time derivative of the inertia matrix $\dot{M}(\boldsymbol{q})$ is a symmetric matrix and satisfies: $\dot{M}(\boldsymbol{q}) = C(\boldsymbol{q},\dot{\boldsymbol{q}})^T + C(\boldsymbol{q},\dot{\boldsymbol{q}})$.

Property 2.5: The centrifugal and Coriolis torques matrix $C(\boldsymbol{q},\dot{\boldsymbol{q}})$ and the time derivative $\dot{M}(\boldsymbol{q})$ of the inertia matrix satisfy: $\frac{1}{2}\dot{\boldsymbol{q}}^{\mathrm{T}}[\dot{M}(\boldsymbol{q}) - 2C(\boldsymbol{q},\dot{\boldsymbol{q}})]\dot{\boldsymbol{q}} = 0, \forall \boldsymbol{q},\dot{\boldsymbol{q}} \in \mathbb{R}^n$. Thus, $\left[\dot{M}(\boldsymbol{q}) - 2C(\boldsymbol{q},\dot{\boldsymbol{q}})\right]$ is a skew-symmetric matrix.

Property 2.6: For robots with revolute joints, there exists a positive constant $k_c > 0$, such that: $\|C(\boldsymbol{q},\boldsymbol{x})\boldsymbol{y}\| \leq k_c\|\boldsymbol{x}\|\|\boldsymbol{y}\|$, $\forall \boldsymbol{q},\boldsymbol{x},\boldsymbol{y} \in \mathbb{R}^n$. Note that, $\|C(\boldsymbol{q},\dot{\boldsymbol{q}})\dot{\boldsymbol{q}}\| \leq k_c\|\dot{\boldsymbol{q}}\|^2$.

Property 2.7: The viscous friction torque $B\dot{\boldsymbol{q}}$ is a dissipate energy that satisfies: $\dot{\boldsymbol{q}}^T B\dot{\boldsymbol{q}} > 0, \forall \dot{\boldsymbol{q}} \neq \boldsymbol{0} \in \mathbb{R}^n$; B is a positive definite diagonal matrix, and $\lambda_B^{\min}\|\dot{\boldsymbol{q}}\|^2 \leq \dot{\boldsymbol{q}}^T B\dot{\boldsymbol{q}} \leq \lambda_B^{\max}\|\dot{\boldsymbol{q}}\|^2$, where $\lambda_B^{\min}, \lambda_B^{\max}$ are maximum and minimum eigenvalues of the viscous friction matrix B, respectively.

Property 2.8: If the robot manipulator has only revolute joints, then the gravitational torque vector $\boldsymbol{g}(\boldsymbol{q})$ is bounded $\forall \boldsymbol{q} \in \mathbb{R}^n$ and there exists a constant k_g such that $\|\boldsymbol{g}(\boldsymbol{q})\| \leq k_g, \forall \boldsymbol{q} \in \mathbb{R}^n$.

3. Properties of the asinh-type control

This section describes the main properties and qualities of the new asinh-type control scheme, which we denote by asinh$(\cdot)$. Our motivation to use this function as control structure is based on the following: This function is a vectorial map, asinh$(\boldsymbol{x}) : \mathbb{R}^n \to \mathbb{R}^n$; being asinh$(\boldsymbol{x}) = \left[\text{asinh}(x_1)\ \cdots\ \text{asinh}(x_n)\right]^{\mathrm{T}}$ continuous in $\boldsymbol{x} \in \mathbb{R}^n$. It is not a bounded function. But it is a monotonically increasing function and located within the first and third quadrants; it is an odd function and symmetric about the origin. It is also approximately linear close to the origin. When $\boldsymbol{x}$ takes large values, its behavior is similar to $\ln(2\boldsymbol{x})$, as shown in Figure 1. As $\boldsymbol{x}$ approaches positive (negative) infinity, asinh$(\boldsymbol{x})$ approaches positive (negative) infinity, respectively. However, its first partial derivative (gradient $(\partial/\partial\boldsymbol{x})$ asinh(x_i), for $i = 1, 2, \ldots, n$) is bounded. Therefore, its growth rate is slower than the PD control and exponential increasing of the hyperbolic functions (sinh and cosh functions). All these qualities represent key elements to design the control structure, as well as tuning the control gains and avoiding the saturation of the servo-amplifiers. The above features are used to drive the position error and to obtain energy dissipation from the derivative term.

Within the group of inverse hyperbolic functions, in addition to the asinh function, there are also the atanh and acosh functions. However, the acosh function is defined only $|x_i| \geq 1$ (at least where real vectors are concerned), for $i = 1, 2, \ldots n$. Its behavior is only in the first quadrant, so it does not return negative values, then this function could not be evaluated as a control scheme.

On the other hand, for the case of the atanh function, it is found in the first and third quadrants

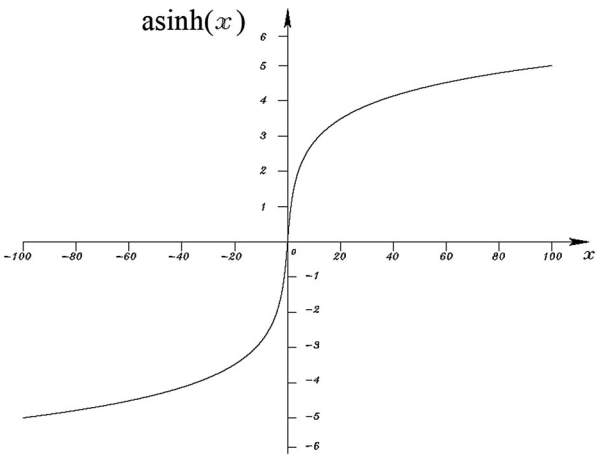

Figure 1. Behavior of the function asinh$(\boldsymbol{x})$.

and it is an odd function, which is symmetric with respect to zero. The atanh-type control scheme $\boldsymbol{\tau}_{\text{atanh}} = \frac{1}{2}\ln((1+x_i)/(1-x_i))$ is defined only for $|x_i(t)| < 1$, for $i = 1, 2, \ldots, n$; when x_i is the ith position error (defined as the difference between the desired position and the robot response), then the range of desired references are limited. When its argument x_i is close to 1, the numerical value of the atanh function grows exponentially, requesting very large torque magnitudes, which is a disadvantage. While the proposed control $\operatorname{asinh}(x_i) = \ln(x_i + \sqrt{x_i^2+1}) \;\; \forall x_i \in \mathbb{R}$, with $i = 1, 2, \ldots, n$, its domain is the whole Euclidean space.

We present some useful mathematical properties of the function $\operatorname{asinh}(\boldsymbol{x})$ which can be used in the stability analysis of the proposed asinh control scheme.

Property 3.1: The Euclidean-norm of the gradient $\partial \operatorname{asinh}(x_i)/\partial x_i$ is bounded, for $i = 1, 2, \ldots, n$, satisfies:

$$\begin{aligned}\left\| \left[\frac{\partial \operatorname{asinh}(x_1)}{\partial x_1} \quad \frac{\partial \operatorname{asinh}(x_2)}{\partial x_2} \quad \cdots \quad \frac{\partial \operatorname{asinh}(x_n)}{\partial x_n} \right]^{\mathrm{T}} \right\| \\ = \left\| \left[\frac{1}{\sqrt{1+x_1^2}} \quad \frac{1}{\sqrt{1+x_2^2}} \quad \cdots \quad \frac{1}{\sqrt{1+x_n^2}} \right]^{\mathrm{T}} \right\| \\ \leq \begin{cases} \sqrt{n}\rho^*, & \forall \boldsymbol{x} \in \mathbb{R}^n \\ \rho^* \|\boldsymbol{x}\|, & \forall \boldsymbol{x} \in \mathbb{R}^n \end{cases} \end{aligned} \tag{3}$$

where ρ^* is a positive constant and represents an upper bound.

Property 3.2: There exist positive numbers $\delta^u, \delta^l \in \mathbb{R}_+$ (see the Shafer-Fink inequalities in [29]), such as:

$$\begin{aligned}(\delta^l + 1) \left\| \frac{\boldsymbol{x}}{\delta^l + \sqrt{1+\boldsymbol{x}^2}} \right\| \leq \|\operatorname{asinh}(\boldsymbol{x})\| \\ \leq (\gamma^u + 1) \left\| \frac{\boldsymbol{x}}{\gamma^u + \sqrt{1+\boldsymbol{x}^2}} \right\| \leq \delta^u \|\boldsymbol{x}\| \end{aligned} \tag{4}$$

where the $n \times 1$ vector

$$\begin{aligned}\frac{(\gamma+1)\boldsymbol{x}}{\gamma + \sqrt{1+\boldsymbol{x}^2}} \\ = \left[\frac{(\gamma+1)x_1}{\gamma + \sqrt{1+x_1^2}}, \frac{(\gamma+1)x_2}{\gamma + \sqrt{1+x_2^2}}, \ldots, \right. \\ \left. \times \frac{(\gamma+1)x_n}{\gamma + \sqrt{1+x_n^2}} \right]^{\mathrm{T}}; \end{aligned}$$

being $\delta^l \in (0, 2]$. We define $\delta^u = \gamma^u + 1$, $\gamma^u \in \mathbb{R}_+$, and considering δ^u as an upper bound. The inequality (4) holds true if and only if

$$\gamma^u \geq \frac{\sqrt{1+\rho^2}\operatorname{asinh}(\rho) - \rho}{\rho - \operatorname{asinh}(\rho)},$$

for all $\rho \in \mathbb{R}_+$ span the interval $0 < \|\boldsymbol{x}\| \leq \rho$.

Property 3.3: Since the function $\operatorname{asinh}(\boldsymbol{x})$ is an odd function, i.e. $\operatorname{asinh}(-\boldsymbol{x}) = -\operatorname{asinh}(\boldsymbol{x})$, then if $\Lambda \in \mathbb{R}^{n\times n}$ is a positive definite diagonal matrix, we obtain:

$$\begin{aligned}\lambda_\Lambda^{\min}(\delta^l + 1) \frac{\|\boldsymbol{x}\|^2}{[\delta^l + \sqrt{1+\|\boldsymbol{x}\|^2}]^2} \\ \leq \boldsymbol{x}^T \Lambda \operatorname{asinh}(\boldsymbol{x}) \leq \delta^u \lambda_\Lambda^{\max} \|\boldsymbol{x}\|^2 \end{aligned} \tag{5}$$

where $\lambda_\Lambda^{\min}$ and $\lambda_\Lambda^{\max}$ are the minimum and maximum eigenvalues of the matrix Λ, respectively.

4. Analysis of global asymptotic stability

This section presents the global asymptotic stability analysis of the new asinh-type control scheme. Given any initial condition $[\boldsymbol{q}(0), \; \dot{\boldsymbol{q}}(0)]^{\mathrm{T}} \in \mathbb{R}^{2n}$, the position control problem for robot manipulators consists in proposing a control scheme such that, the applied torque $\boldsymbol{\tau} \in \mathbb{R}^n$ to robot joints $\boldsymbol{q}(t)$ tend asymptotically to a constant desired joint position $\boldsymbol{q}_d \in \mathbb{R}^n$, that is: $\lim_{t\to\infty} \begin{bmatrix} \tilde{\boldsymbol{q}}(t) \\ \dot{\boldsymbol{q}}(t) \end{bmatrix} \to \boldsymbol{0} \in \mathbb{R}^{2n}$, $\forall t \geq 0$, where $\tilde{\boldsymbol{q}} \in \mathbb{R}^n$ is the joint position error, which is defined as $\tilde{\boldsymbol{q}} = \boldsymbol{q}_d - \boldsymbol{q}(t)$.

To resolve the position control problem, we propose a control structure $\boldsymbol{\tau}$ composed by functions $\operatorname{asinh}(\cdot)$ to drive both the position error and derivative action terms, plus a component of gravity compensation. Consider the following control scheme, given by

$$\boldsymbol{\tau} = K_p \operatorname{asinh}(\tilde{\boldsymbol{q}}) - K_v \operatorname{asinh}(\dot{\boldsymbol{q}}) + \boldsymbol{g}(\boldsymbol{q}) \tag{6}$$

where $\operatorname{asinh}(\tilde{\boldsymbol{q}}), \operatorname{asinh}(\dot{\boldsymbol{q}}) \in \mathbb{R}^n$ represent the proportional and derivative control terms, respectively. These terms play similar qualitative roles as the P and D control actions for the linear PD case. In other words, the term $K_p \operatorname{asinh}(\tilde{\boldsymbol{q}})$ acts like a virtual nonlinear spring that tries to restore each link to the desired set point, and the derivative action $-K_v \operatorname{asinh}(\dot{\boldsymbol{q}})$ has a behavior similar to a virtual nonlinear damper that dissipates the motion generated by the velocity $\dot{\boldsymbol{q}}$, consequently opposes to motion. The proportional and derivative control gains are denoted by $K_p, K_v \in \mathbb{R}^{n\times n}$, respectively. Both gains are positive definite diagonal matrices, and $\boldsymbol{\tau} \in \mathbb{R}^n$ is the vector of applied torques.

The closed-loop system equation is obtained by combining the robot dynamics model (1) and the control law (6) as follows:

$$\frac{\mathrm{d}}{\mathrm{d}t} \begin{bmatrix} \tilde{\boldsymbol{q}} \\ \dot{\boldsymbol{q}} \end{bmatrix} = \begin{bmatrix} -\dot{\boldsymbol{q}} \\ M^{-1}(\boldsymbol{q}_d - \tilde{\boldsymbol{q}})[K_p \operatorname{asinh}(\tilde{\boldsymbol{q}}) - K_v \operatorname{asinh}(\dot{\boldsymbol{q}}) \\ -B\dot{\boldsymbol{q}} - C(\boldsymbol{q}_d - \tilde{\boldsymbol{q}}, \dot{\boldsymbol{q}})\dot{\boldsymbol{q}}] \end{bmatrix} \tag{7}$$

which is an autonomous nonlinear differential equation. In order to demonstrate that the state origin is the unique equilibrium point, it is necessary to consider the Properties 2.1 and 2.7 on the matrices $M(\boldsymbol{q}_d - \tilde{\boldsymbol{q}})$

and B, respectively. The diagonal positive definite diagonal matrices K_p and K_v are proposed by the user. The following assumptions are taken into account:

(a) The first component of (7) satisfies $-\dot{\boldsymbol{q}} = -I\dot{\boldsymbol{q}} = \mathbf{0} \Leftrightarrow \dot{\boldsymbol{q}} = \mathbf{0}$, due to the fact that $I \in \mathbb{R}^{n\times n}$ is the identity matrix.
(b) For the second component in (7), we use the Property 2.1 of the inertia matrix and its inverse matrix are positive definite matrices. Since $\dot{\boldsymbol{q}} = \mathbf{0} \in \mathbb{R}^n$ the derivative control action satisfies: $K_v \operatorname{asinh}(\dot{\boldsymbol{q}}) = \mathbf{0} \in \mathbb{R}^n \Longleftrightarrow \dot{\boldsymbol{q}} = \mathbf{0} \in \mathbb{R}^n$. Also, $B\dot{\boldsymbol{q}} = \mathbf{0} \in \mathbb{R}^n \Longleftrightarrow \dot{\boldsymbol{q}} = \mathbf{0} \in \mathbb{R}^n$. Using property (2.3), the vector of centripetal and Coriolis torques is the zero vector. Thus, $\operatorname{asinh}(\tilde{\boldsymbol{q}}) = \mathbf{0} \Longleftrightarrow \tilde{\boldsymbol{q}} = \mathbf{0} \in \mathbb{R}^n$.

Therefore, the state origin $\left[\tilde{\boldsymbol{q}},\ \dot{\boldsymbol{q}}\right]^{\mathrm{T}} = \mathbf{0} \in \mathbb{R}^{2n}$ exists and it is the unique equilibrium point of the dynamic system (7).

Proposition 4.1: *Consider the robot dynamics model* (1) *together with the control structure* (6), *then equilibrium point* $[\tilde{\boldsymbol{q}},\ \dot{\boldsymbol{q}}]^{\mathrm{T}} = \mathbf{0} \in \mathbb{R}^{2n}$ *of the closed-loop system* (7) *is globally asymptotically stable in joint space.*

Proof: To carry out the stability analysis, we propose the following Lyapunov function candidate composed by the sum of the robot manipulator kinetic energy, artificial potential energy, plus a cross-term between position error and velocity:

$$
\begin{aligned}
&V(\dot{\boldsymbol{q}}, \tilde{\boldsymbol{q}}) \\
&\quad = \frac{1}{2}\dot{\boldsymbol{q}}^T M(\boldsymbol{q}_d - \tilde{\boldsymbol{q}})\dot{\boldsymbol{q}} \\
&\qquad + \left[\sqrt{\tilde{\boldsymbol{q}}\operatorname{asinh}(\tilde{\boldsymbol{q}}) - \sqrt{\tilde{\boldsymbol{q}}^2 + 1} + 1}\right]^{\mathrm{T}} K_p \\
&\qquad \times \left[\sqrt{\tilde{\boldsymbol{q}}\operatorname{asinh}(\tilde{\boldsymbol{q}}) - \sqrt{\tilde{\boldsymbol{q}}^2 + 1} + 1}\right] \\
&\qquad - \frac{\epsilon_0}{1 + \|\tilde{\boldsymbol{q}}\|}\operatorname{asinh}(\tilde{\boldsymbol{q}})^T M(\boldsymbol{q}_d - \tilde{\boldsymbol{q}})\dot{\boldsymbol{q}} \\
&\qquad + \frac{1}{2}\frac{\epsilon_0^2}{[1 + \|\tilde{\boldsymbol{q}}\|]^2}\operatorname{asinh}(\tilde{\boldsymbol{q}})^T M(\boldsymbol{q}_d - \tilde{\boldsymbol{q}})\operatorname{asinh}(\tilde{\boldsymbol{q}})
\end{aligned}
\tag{8}
$$

where ϵ_0 is any positive number. It is important to note that ϵ_0 is only required for purposes of analysis, and therefore, we do not need to know its numerical value. Just it is needed to prove that it exists.

For simplicity, from (8) for the vector $\sqrt{\tilde{\boldsymbol{q}}\operatorname{asinh}(\tilde{\boldsymbol{q}}) - \sqrt{\tilde{\boldsymbol{q}}^2 + 1} + 1}$, we have used the following notation:

$$
\begin{aligned}
&\sqrt{\tilde{\boldsymbol{q}}\operatorname{asinh}(\tilde{\boldsymbol{q}}) - \sqrt{\tilde{\boldsymbol{q}}^2 + 1} + 1} \\
&\quad = \left[\sqrt{\tilde{q}_1\operatorname{asinh}(\tilde{q}_1) - \sqrt{\tilde{q}_1^2 + 1} + 1},\ \ldots,\right. \\
&\qquad \left.\times \sqrt{\tilde{q}_n\operatorname{asinh}(\tilde{q}_n) - \sqrt{\tilde{q}_n^2 + 1} + 1}\right]^{\mathrm{T}} \in \mathbb{R}^n.
\end{aligned}
$$

On the other hand, a strict Lyapunov function is a globally positive-definite function, whose time derivative along the trajectories of the closed-loop system (7) yields a globally negative-definite function. Then Lyapunov's direct method allows to conclude global asymptotic stability, avoiding to use the Krasovskii-LaSalle theorem. For the sake of completeness, we provide an outline of the proof that the Lyapunov function candidate (8) is a positive-definite function. It can be rewritten as follows:

$$
\begin{aligned}
V(\dot{\boldsymbol{q}}, \tilde{\boldsymbol{q}}) &= \frac{1}{2}\left[\dot{\boldsymbol{q}} - \frac{\epsilon_0}{1 + \|\tilde{\boldsymbol{q}}\|}\operatorname{asinh}(\tilde{\boldsymbol{q}})\right]^{\mathrm{T}} M(\boldsymbol{q}_d - \tilde{\boldsymbol{q}}) \\
&\quad \times \left[\dot{\boldsymbol{q}} - \frac{\epsilon_0}{1 + \|\tilde{\boldsymbol{q}}\|}\operatorname{asinh}(\tilde{\boldsymbol{q}})\right] \\
&\quad + \left[\sqrt{\tilde{\boldsymbol{q}}\operatorname{asinh}(\tilde{\boldsymbol{q}}) - \sqrt{\tilde{\boldsymbol{q}}^2 + 1} + 1}\right]^{\mathrm{T}} K_p \\
&\quad \times \left[\sqrt{\tilde{\boldsymbol{q}}\operatorname{asinh}(\tilde{\boldsymbol{q}}) - \sqrt{\tilde{\boldsymbol{q}}^2 + 1} + 1}\right]
\end{aligned}
\tag{9}
$$

Since $M(\boldsymbol{q}_d - \tilde{\boldsymbol{q}})$ is a positive definite matrix by Property 2.1, the first term of (9) is radially unbounded and a positive definite function for $\dot{\boldsymbol{q}}$ and $\tilde{\boldsymbol{q}}$ for any $\epsilon_0 > 0$. Similarly for the second term, which is also positive definite in the variable $\tilde{\boldsymbol{q}}$, because K_p is a positive definite diagonal matrix.

Now, we proceed to obtain the time derivative of the Lyapunov function candidate (8) along the trajectories of the closed-loop equation (7). Substituting the acceleration joint vector $\ddot{\boldsymbol{q}}$ from closed-loop equation (7), we get:

$$
\begin{aligned}
&\dot{V}(\dot{\boldsymbol{q}}, \tilde{\boldsymbol{q}}) \\
&\quad = \dot{\boldsymbol{q}}^T K_p \operatorname{asinh}(\tilde{\boldsymbol{q}}) - \dot{\boldsymbol{q}}^T K_v \operatorname{asinh}(\dot{\boldsymbol{q}}) - \dot{\boldsymbol{q}}^T B\dot{\boldsymbol{q}} \\
&\qquad - \dot{\boldsymbol{q}}^T C(\boldsymbol{q}, \dot{\boldsymbol{q}})\dot{\boldsymbol{q}} + \frac{1}{2}\dot{\boldsymbol{q}}^T \dot{M}(\boldsymbol{q})\dot{\boldsymbol{q}} - \dot{\boldsymbol{q}}^T K_p \operatorname{asinh}(\tilde{\boldsymbol{q}}) \\
&\qquad + \frac{\epsilon_0}{1 + \|\tilde{\boldsymbol{q}}\|}\left[\frac{\dot{\boldsymbol{q}}}{\sqrt{1 + \tilde{\boldsymbol{q}}^2}}\right]^{\mathrm{T}} M(\boldsymbol{q}_d - \tilde{\boldsymbol{q}})\dot{\boldsymbol{q}} \\
&\qquad - \epsilon_0 \frac{\tilde{\boldsymbol{q}}^T \dot{\boldsymbol{q}}}{\|\tilde{\boldsymbol{q}}\|[1 + \|\tilde{\boldsymbol{q}}\|]^2}\operatorname{asinh}(\tilde{\boldsymbol{q}})^T M(\boldsymbol{q}_d - \tilde{\boldsymbol{q}})\dot{\boldsymbol{q}} \\
&\qquad - \frac{\epsilon_0}{1 + \|\tilde{\boldsymbol{q}}\|}\operatorname{asinh}(\tilde{\boldsymbol{q}})^T \dot{M}(\boldsymbol{q}_d - \tilde{\boldsymbol{q}})\dot{\boldsymbol{q}} \\
&\qquad - \frac{\epsilon_0}{1 + \|\tilde{\boldsymbol{q}}\|}\operatorname{asinh}(\tilde{\boldsymbol{q}})^T K_p \operatorname{asinh}(\tilde{\boldsymbol{q}})^T \\
&\qquad + \frac{\epsilon_0}{1 + \|\tilde{\boldsymbol{q}}\|}\operatorname{asinh}(\tilde{\boldsymbol{q}})^T B\dot{\boldsymbol{q}} \\
&\qquad + \frac{\epsilon_0}{1 + \|\tilde{\boldsymbol{q}}\|}\operatorname{asinh}(\tilde{\boldsymbol{q}})^T K_v \operatorname{asinh}(\dot{\boldsymbol{q}})
\end{aligned}
$$

$$+\frac{\epsilon_0}{1+\|\tilde{\boldsymbol{q}}\|}\operatorname{asinh}(\tilde{\boldsymbol{q}})^T C(\boldsymbol{q}_d-\tilde{\boldsymbol{q}},\dot{\boldsymbol{q}})\dot{\boldsymbol{q}}$$
$$+\frac{\epsilon_0^2}{[1+\|\tilde{\boldsymbol{q}}\|]^2}\operatorname{asinh}(\tilde{\boldsymbol{q}})^T\dot{M}(\boldsymbol{q})\operatorname{asinh}(\tilde{\boldsymbol{q}})$$
$$-\frac{\epsilon_0^2}{2[1+\|\tilde{\boldsymbol{q}}\|]^2}\left[\frac{\dot{\boldsymbol{q}}}{\sqrt{1+\tilde{\boldsymbol{q}}^2}}\right]^{\mathrm{T}}$$
$$\times M(\boldsymbol{q}_d-\tilde{\boldsymbol{q}})\operatorname{asinh}(\tilde{\boldsymbol{q}})$$
$$+\frac{\epsilon_0^2\tilde{\boldsymbol{q}}^T\dot{\boldsymbol{q}}}{2\|\tilde{\boldsymbol{q}}\|[1+\|\tilde{\boldsymbol{q}}\|]^3}\operatorname{asinh}(\tilde{\boldsymbol{q}})^T$$
$$\times M(\boldsymbol{q}_d-\tilde{\boldsymbol{q}})\operatorname{asinh}(\tilde{\boldsymbol{q}}) \tag{10}$$

we use the following notation to represent the vector

$$\left[\frac{\dot{\boldsymbol{q}}}{\sqrt{1+\tilde{\boldsymbol{q}}^2}}\right]=\left[\frac{\dot{q}_1}{\sqrt{1+\tilde{q}_1^2}},\cdots,\frac{\dot{q}_n}{\sqrt{1+\tilde{q}_n^2}}\right]^{\mathrm{T}}\in\mathbb{R}^n.$$

Cancellation of some terms on its right-hand side of the equation (10) is made to simplify it. For example, the first and sixth terms are canceled; using the Property 2.5 of the skew-matrix on the fourth and fifth terms produces a zero term. Note that, in the ninth term, we use the Property 2.4, $\dot{M}(\boldsymbol{q}_d-\tilde{\boldsymbol{q}})$, which has been replaced by its equivalent expression. Therefore, it is canceled with the thirteenth term. The same Property 2.4 is also used in the fourteenth term, then we get:

$$\dot{V}(\dot{\boldsymbol{q}},\tilde{\boldsymbol{q}})=-\dot{\boldsymbol{q}}^T K_v\operatorname{asinh}(\dot{\boldsymbol{q}})-\dot{\boldsymbol{q}}^T B\dot{\boldsymbol{q}}$$
$$+\frac{\epsilon_0}{1+\|\tilde{\boldsymbol{q}}\|}\left[\frac{\dot{\boldsymbol{q}}}{\sqrt{1+\tilde{\boldsymbol{q}}^2}}\right]^{\mathrm{T}}M(\boldsymbol{q}_d-\tilde{\boldsymbol{q}})\dot{\boldsymbol{q}}$$
$$-\epsilon_0\frac{\tilde{\boldsymbol{q}}^T\dot{\boldsymbol{q}}}{\|\tilde{\boldsymbol{q}}\|[1+\|\tilde{\boldsymbol{q}}\|]^2}\operatorname{asinh}(\tilde{\boldsymbol{q}})^T M(\boldsymbol{q}_d-\tilde{\boldsymbol{q}})\dot{\boldsymbol{q}}$$
$$-\frac{\epsilon_0}{1+\|\tilde{\boldsymbol{q}}\|}\operatorname{asinh}(\tilde{\boldsymbol{q}})^T K_p\operatorname{asinh}(\tilde{\boldsymbol{q}})$$
$$+\frac{\epsilon_0}{1+\|\tilde{\boldsymbol{q}}\|}\operatorname{asinh}(\tilde{\boldsymbol{q}})^T B\dot{\boldsymbol{q}}$$
$$+\frac{\epsilon_0}{1+\|\tilde{\boldsymbol{q}}\|}\operatorname{asinh}(\tilde{\boldsymbol{q}})^T K_v\operatorname{asinh}(\dot{\boldsymbol{q}})$$
$$+\frac{\epsilon_0}{1+\|\tilde{\boldsymbol{q}}\|}\operatorname{asinh}(\tilde{\boldsymbol{q}})^T C^T(\boldsymbol{q}_d-\tilde{\boldsymbol{q}},\dot{\boldsymbol{q}})\dot{\boldsymbol{q}}$$
$$+\frac{\epsilon_0^2}{[1+\|\tilde{\boldsymbol{q}}\|]^2}\operatorname{asinh}(\tilde{\boldsymbol{q}})^T$$
$$\times\left[C(\boldsymbol{q}_d-\tilde{\boldsymbol{q}},\dot{\boldsymbol{q}})+C^T(\boldsymbol{q}_d-\tilde{\boldsymbol{q}},\dot{\boldsymbol{q}})\right]\operatorname{asinh}(\tilde{\boldsymbol{q}})$$
$$-\frac{\epsilon_0^2}{2[1+\|\tilde{\boldsymbol{q}}\|]^2}\left[\frac{\dot{\boldsymbol{q}}}{\sqrt{1+\tilde{\boldsymbol{q}}^2}}\right]^{\mathrm{T}}$$
$$\times M(\boldsymbol{q}_d-\tilde{\boldsymbol{q}})\operatorname{asinh}(\tilde{\boldsymbol{q}})$$
$$+\frac{\epsilon_0^2\tilde{\boldsymbol{q}}^T\dot{\boldsymbol{q}}}{2\|\tilde{\boldsymbol{q}}\|[1+\|\tilde{\boldsymbol{q}}\|]^3}\operatorname{asinh}(\tilde{\boldsymbol{q}})^T$$
$$\times M(\boldsymbol{q}_d-\tilde{\boldsymbol{q}})\operatorname{asinh}(\tilde{\boldsymbol{q}}) \tag{11}$$

Now, we proceed to obtain upper bounds of all terms of Lyapunov function (11). Observe that from Property (3.1), the Euclidean-norm of the vector $[\dot{\boldsymbol{q}}/\sqrt{1+\tilde{\boldsymbol{q}}^2}]$ satisfies: $\|\dot{\boldsymbol{q}}/\sqrt{1+\tilde{\boldsymbol{q}}^2}\|\leq\sqrt{n}\rho^*\|\dot{\boldsymbol{q}}\|$. We also use the inequalities (3) and (5) from Properties 2.2, 2.6 and 2.7. After performing grouping algebraic and reduction of terms, equation (11) can be rewritten as

$$\dot{V}(\dot{\boldsymbol{q}},\tilde{\boldsymbol{q}})\leq-\Bigg[\lambda_B^{\min}-\Big[(\delta_v^u+1)\lambda_{K_v}^{\max}$$
$$+\frac{\epsilon_0}{1+\|\tilde{\boldsymbol{q}}\|}(\sqrt{n}\rho^*\beta_M$$
$$+(\delta_p^u+1)(\beta_M+k_c))\Big]\Bigg]\|\dot{\boldsymbol{q}}\|^2$$
$$+\frac{\epsilon_0}{1+\|\tilde{\boldsymbol{q}}\|}(\delta_p^u+1)\Big[\lambda_B^{\max}+\lambda_{K_v}^{\max}$$
$$+\epsilon_0(2k_c(\delta_p^u+1)+(\delta_p^u+2)\beta_M)\Big]\|\tilde{\boldsymbol{q}}\|\|\dot{\boldsymbol{q}}\|$$
$$-\frac{\epsilon_0}{1+\|\tilde{\boldsymbol{q}}\|}\frac{(\delta_p^l+1)^2\lambda_{K_p}^{\min}}{\left[\delta_p^l+\sqrt{1+\|\tilde{\boldsymbol{q}}\|^2}\right]^4}\|\tilde{\boldsymbol{q}}\|^2 \tag{12}$$

where $\delta_p^u,\delta_v^u\in\mathbb{R}_+$ are positive numbers that satisfy the upper inequality (4) of the Properties 3.2 and 3.3 for the proportional and derivative terms of the proposed control scheme (6), respectively. While, $\delta_p^l\in\mathbb{R}_+$ satisfies the lower inequality (4) from Properties 3.2 and 3.3 for the proportional term of the control algorithm (6). The minimum and maximum eigenvalues of the gains K_p and K_v are represented by $\lambda_{K_p}^{\min},\lambda_{K_v}^{\min}\in\mathbb{R}_+$ and $\lambda_{K_p}^{\max},\lambda_{K_v}^{\max}\in\mathbb{R}_+$, respectively.

The previous upper bounds yield that the time derivative $\dot{V}(\dot{\boldsymbol{q}},\tilde{\boldsymbol{q}})$ in (12) can be expressed as

$$\dot{V}(\dot{\boldsymbol{q}},\tilde{\boldsymbol{q}})<-\begin{bmatrix}\|\tilde{\boldsymbol{q}}\|\\\|\dot{\boldsymbol{q}}\|\end{bmatrix}^{\mathrm{T}}\underbrace{\begin{bmatrix}\phi_{11}&\phi_{12}\\\phi_{21}&\phi_{22}\end{bmatrix}}_{\Phi}\begin{bmatrix}\|\tilde{\boldsymbol{q}}\|\\\|\dot{\boldsymbol{q}}\|\end{bmatrix}$$

where the components of the matrix $\Phi\in\mathbb{R}^{2\times2}$ are given by

$$\phi_{11}=\frac{\epsilon_0}{1+\|\tilde{\boldsymbol{q}}\|}\frac{(\delta_p^l+1)^2\lambda_{K_p}^{\min}}{\left[\delta_p^l+\sqrt{1+\|\tilde{\boldsymbol{q}}\|^2}\right]^4} \tag{13a}$$

$$\phi_{12}=\phi_{21}=-\frac{1}{2}\frac{\epsilon_0}{1+\|\tilde{\boldsymbol{q}}\|}(\delta_p^u+1)\Big[\lambda_B^{\max}+\lambda_{K_v}^{\max}$$
$$+\epsilon_0[2k_c(\delta_p^u+1)+\beta_M(\delta_p^u+2)]\Big] \tag{13b}$$

$$\phi_{22}=\lambda_B^{\min}-\Bigg[(\delta_v^u+1)\lambda_{K_v}^{\max}+\frac{\epsilon_0}{1+\|\tilde{\boldsymbol{q}}\|}(\sqrt{n}\rho^*\beta_M$$
$$+(\delta_p^u+1)(\beta_M+k_c))\Bigg] \tag{13c}$$

In order to ensure that Φ is a positive definite matrix, the element ϕ_{11} must be positive. This condition is satisfied due to that all constants $\epsilon_0,\delta_p^l,\lambda_{K_p}^{\min}$ are positive

numbers. The determinant $\det[\Phi]$ of the matrix Φ is positive in the interval Ω,

$$\Omega = \min \left\{ \begin{array}{c} \dfrac{\dfrac{(\delta_p^l+1)^2\lambda_{Kp}^{\min}}{\left[\delta_p^l+\sqrt{1+\|\tilde{\boldsymbol{q}}\|^2}\right]^4}\left[\lambda_B^{\min}-(\delta_v^u+1)\lambda_{K_v}^{\max}\right]}{\dfrac{(\delta_p^l+1)^2\lambda_{Kp}^{\min}}{\left[\delta_p^l+\sqrt{1+\|\tilde{\boldsymbol{q}}\|^2}\right]^4}\left[\sqrt{n}\rho^*\beta_M+(\delta_p^u+1)(\beta_M+k_c)\right]+\frac{1}{4}(\delta_p^u+1)^2(\lambda_B^{\max}+\lambda_{K_v}^{\max})^2}, \\ \dfrac{\dfrac{(\delta_p^l+1)\sqrt{\lambda_{Kp}^{\min}}}{\left[\delta_p^l+\sqrt{1+\|\tilde{\boldsymbol{q}}\|^2}\right]^2}\sqrt{\left[\lambda_B^{\min}-(\delta_v^u+1)\lambda_{K_v}^{\max}\right]}}{\dfrac{\frac{1}{\sqrt{2}}(\delta_p^u+1)\sqrt{\lambda_B^{\max}+\lambda_{K_v}^{\max}}}{\sqrt{\sqrt{n}\rho^*\beta_M+(\delta_p^u+1)(\beta_M+k_c)}}}, \\ \dfrac{\dfrac{(\delta_p^l+1)^{2/3}\lambda_{Kp}^{\min 2/3}}{\left[\delta_p^l+\sqrt{1+\|\tilde{\boldsymbol{q}}\|^2}\right]^{2/3}}\left[\lambda_B^{\min}-(\delta_v^u+1)\lambda_{K_v}^{\max}\right]^{2/3}}{\frac{1}{4^{1/3}}(\delta_p^u+1)^{2/3}(\sqrt{n}\rho^*\beta_M+(\delta_p^u+1)(\beta_M+k_c))^{2/3}} \end{array} \right\}$$

$$> \frac{\epsilon_0}{1+\|\tilde{\boldsymbol{q}}\|} > 0 \tag{14}$$

To complete the proof, observe that inequality (14) is only sufficient to hold for any ϵ_0:

$$\frac{\lambda_B^{\min}}{\delta_v^u+1} > \lambda_{K_v}^{\max} > 0 \tag{15}$$

Thus, $\dot{V}(\dot{\boldsymbol{q}},\tilde{\boldsymbol{q}})$ is a negative definite function. It is worth mentioning that since both conditions $V(\dot{\boldsymbol{q}},\tilde{\boldsymbol{q}}) > 0$ and $\dot{V}(\dot{\boldsymbol{q}},\tilde{\boldsymbol{q}}) < 0$ are satisfied, then the proposed Lyapunov function candidate is a strict Lyapunov function. Consequently, the existence of a positive number ϵ_0 is ensured fulfilling inequality (14). Therefore, according to Lyapunov's direct method, we conclude asymptotic stability of the origin $\left[\tilde{\boldsymbol{q}},\dot{\boldsymbol{q}}\right]^{\mathrm{T}} = \mathbf{0} \in \mathbb{R}^{2n}$ of the closed-loop equation (7). In other words, $\tilde{\boldsymbol{q}}(t)$ and $\dot{\boldsymbol{q}}(t)$ asymptotically converge to zero, as $t \longrightarrow \infty$. This completes the proof. ■

5. Experimental setup

To support our theoretical developments, this section describes the robot manipulator setup and the experimental results of the evaluated control schemes. The experimental system is a direct-drive 3-dof robot arm moving in three-dimensional space, whose workspace is a sphere with radius of 1 m, as it is shown in Figure 2. The arm links are made of 6061 aluminum actuated by brushless direct-drive servomotors from Parker Compumotor to drive the robot joints without gear reduction. Advantages of this type of direct-drive actuators include freedom from backslash, significantly lower friction phenomena compared with actuators composed by gear drives, and they work as an ideal source of applied torque when they are operated in torque mode. The servomotor models used in the experimental robot are listed in Table 1. The position information $\boldsymbol{q}$ is obtained from their incremental encoders and the velocity signals $\dot{\boldsymbol{q}}$ from standard backwards difference algorithm applied to the position joint measurements. The electronic interface of the robot manipulator is composed by a motion control board. It is the PMDi LC228 model manufactured by Precision MicroDynamic Inc. The real-time evaluated control algorithms have been written in C language, and the sampling rate was executed at 2.5 ms on a Pentium-type host computer.

Figure 2. Experimental robot manipulator.

Table 1. Servo actuators of the experimental robot.

Link	Model	Torque [Nm]	Enconder [p/rev]
Base	DR1060B60	60	1,638,400
Shoulder	DR1100D100	100	1,015,808
Elbow	DM1004C	4	2,621,440

6. Experimental results

The experimental results consist in studying the robot's behavior by moving it from an initial position to a fixed desired configuration. The experiments consist of two phases. The first one studies the performance of control schemes for a fixed set-point $\boldsymbol{q}_d = \left[\frac{\pi}{4}, \frac{\pi}{4}, \frac{\pi}{4}\right]^{\mathrm{T}}$ rad. The second part is to generate a set of random numbers as set-points. The two experimental phases are carried

out with the same tuning of control gains. An experimental comparison is made between the following control schemes: PD [3], atanh and asinh algorithms, which have been defined as $\boldsymbol{\tau}_{\mathrm{PD}}$, $\boldsymbol{\tau}_{\mathrm{atanh}}$ and $\boldsymbol{\tau}_{\mathrm{asinh}}$, respectively:

$$\boldsymbol{\tau}_{\mathrm{PD}} = K_p\tilde{\boldsymbol{q}} - K_v\dot{\boldsymbol{q}} + \boldsymbol{g}(\boldsymbol{q}) \tag{16a}$$

$$\boldsymbol{\tau}_{\mathrm{atanh}} = K_p\mathrm{atanh}(\tilde{\boldsymbol{q}}) - K_v\,\mathrm{atanh}(\dot{\boldsymbol{q}}) + \boldsymbol{g}(\boldsymbol{q}) \tag{16b}$$

$$\boldsymbol{\tau}_{\mathrm{asinh}} = K_p\mathrm{asinh}(\tilde{\boldsymbol{q}}) - K_v\mathrm{asinh}(\dot{\boldsymbol{q}}) + \boldsymbol{g}(\boldsymbol{q}) \tag{16c}$$

The gravitational vector $\boldsymbol{g}(\boldsymbol{q})$ is required in the control schemes: $\boldsymbol{g}(\boldsymbol{q}) = \left[g_1(\boldsymbol{q}),\ g_2(\boldsymbol{q}),\ g_3(\boldsymbol{q})\right]^{\mathrm{T}}$, where $g_1(\boldsymbol{q}) = 0$, $g_2(\boldsymbol{q}) = 1.0938\sin(q_2+q_3) + 0.0667\cos(q_2+q_3) + 10.915\sin(q_2) - 0.2025\cos(q_2)$, and $g_3(\boldsymbol{q}) = 1.0938\sin(q_2+q_3) + 0.0667\cos(q_2+q_3)$. Note that from Property 2.8, $|g_2(\boldsymbol{q})| < 12.07$ Nm and $|g_3(\boldsymbol{q})| < 1.16$ Nm. To avoid saturation in the servomotors, the maximum torque of the control schemes for each ith joint (with $i = 1,\ 2,\ 3$) must keep the following restrictions: $|\tau_1| \leq 60$ Nm, $|\tau_2| \leq 100 - 12.07 = 87.93$ Nm and $|\tau_3| \leq 4 - 1.16 = 2.84$ Nm, corresponding to base, shoulder and elbow joints, respectively.

The initial conditions for all experiments are set as: $\boldsymbol{q}(0) = \boldsymbol{0} \in \mathbb{R}^3$, then $\tilde{\boldsymbol{q}}(0) = \boldsymbol{q}_d \in \mathbb{R}^3$ and $\dot{\boldsymbol{q}}(0) = \boldsymbol{0} \in \mathbb{R}^3$. The experiment results lasted 5 s. However, in order to expand the details of the transitory state, the position errors and applied torques are plotted to 1.5 s.

To measure the performance of control algorithms, the scalar–valued $\mathcal{L}^2[\tilde{\boldsymbol{q}}]$ norm of the position error is used. A small $\mathcal{L}^2$ norm represents smaller position error and thus a better performance [30]. A critical part in the experimental evaluation of control algorithms is the tuning of the gains, so the PSO technique, which has been successfully applied in many applications. For example, control gains tuned by PSO is an interesting proposal in Robotics [31–34].

6.1. PSO-based-tuning for the control gains

PSO [31], is inspired by social behavior of animals like ants and birds. PSO is a population based scheme which contains a set of swarm solutions called particles. This scheme is an optimization problem, where each particle has a position in a multidimensional search space, which contains all possible solutions within optimization problem. The PSO algorithm searches for the optimum solution among these possible solutions. Nowadays, the original PSO algorithm has been systematically improved [32–34].

The PSO algorithm is initialized to a group of random particles via iteration to find the optimal solution, by tracking individual best position and group best position to adjust its ith current position $\boldsymbol{x}_i^j \in \mathbb{R}^{i\times d}$ and the speed of the particles to the target area, where jth is the iteration and d is the dimension. Each ith particle has a position defined in the search space for $i = 1, 2, \ldots, n_p$, where n_p is the number of particles with respect to dth dimension of the search space. In order to tune the control gains, the particles $\boldsymbol{x}_i^j$ represent the proportional and derivative control gains on a 6-dimensional search space in the PSO algorithm. Each $\boldsymbol{x}_i^j$ in the search space is a candidate that characterizes the control gains, and this solution candidate is represented by $\boldsymbol{x}_i^j = \left[k_{p_{i1}}^j, k_{p_{i2}}^j, k_{p_{i3}}^j, k_{v_{i1}}^j, k_{v_{i2}}^j, k_{v_{i3}}^j\right] \in \mathbb{R}^{i\times 6}$, where $k_{p_{i1}}^j, k_{p_{i2}}^j, k_{p_{i3}}^j$ and $k_{v_{i1}}^j, k_{v_{i2}}^j, k_{v_{i3}}^j$ are the components of the proportional and derivative control gains for the base, shoulder, elbow joints, respectively. The proportional and derivative matrices are $K_p = \mathrm{diag}\{k_{p_1}, k_{p_2}, k_{p_3}\}$ and $K_v = \mathrm{diag}\{k_{v_1}, k_{v_2}, k_{v_3}\}$. Their corresponding velocities are defined as $\boldsymbol{v}_i^j = [\boldsymbol{v}_{p_{i1}}^j,\ \boldsymbol{v}_{p_{i2}}^j,\ \boldsymbol{v}_{p_{i3}}^j, \boldsymbol{v}_{v_{i1}}^j, \boldsymbol{v}_{v_{i2}}^j, \boldsymbol{v}_{v_{i3}}^j]$.

We have used the mathematical model for motion of particles and updating their position described by [34]. The velocity $\boldsymbol{v}_i^j \in \mathbb{R}^{i\times 6}$ and position $\boldsymbol{x}_i^j \in \mathbb{R}^{i\times 6}$ of each particle in the next iteration j are given by:

$$\boldsymbol{v}_i^{j+1} = w\boldsymbol{v}_i^j + c_1\varsigma_1[\boldsymbol{x}_i^{\mathrm{best}} - \boldsymbol{x}_i^j] + c_2\varsigma_2[\boldsymbol{x}_{gd}^{\mathrm{best}} - \boldsymbol{x}_i^j] \tag{17a}$$

$$\boldsymbol{x}_i^{j+1} = \boldsymbol{x}_i^j + \boldsymbol{v}_i^{j+1} \tag{17b}$$

where $\boldsymbol{x}_i^{\mathrm{best}}$ is the individual best position of the ith particle $\boldsymbol{x}_i^j$, and $\boldsymbol{x}^{\mathrm{best}_{gd}}$ is the global best position of the ith particle $\boldsymbol{x}_i^j$. The acceleration constant c_1 is called cognitive parameter, pulls each particle (proportional and derivative gains) towards the local best position, and constant c_2 called social parameter, pulls the particle towards global best position; w represents the swarm weight or the inertia factor. With constrained factor [33], these constants take the form: $c_1 = \chi\phi_1$, $c_2 = \chi\phi_2, w = \chi$, being $\phi_1 = \phi_2 = 2.05, \phi = \phi_1 + \phi_2$, $\kappa = 1$, $\chi = 2\kappa/|2 - \phi - \sqrt{\phi^2 - 4\phi}|$, $\varsigma_1,\ \varsigma_2 \in [0, 1]$ random numbers as learning factor for individual particle.

PSO is based on the operation of the system state. It adjusts the proportional and derivative particles search target space range with the following minimum and maximum limits $\boldsymbol{x}_i^j(t) \in [\boldsymbol{x}_{\min}, \boldsymbol{x}_{\max}]$, $\boldsymbol{x}_{\min} = [k_{p_{1_{\min}}}, k_{p_{2_{\min}}}, k_{p_{3_{\min}}}, k_{v_{1_{\min}}}, k_{v_{2_{\min}}}, k_{v_{3_{\min}}}]$, $\boldsymbol{x}_{\max} = [k_{p_{1_{\max}}}, k_{p_{2_{\max}}}, k_{p_{3_{\max}}}, k_{v_{1_{\max}}}, k_{v_{2_{\max}}}, k_{v_{3_{\max}}}]$, respectively. The minimum values of the proportional gains have been set as $[k_{p_{1_{\min}}}, k_{p_{2_{\min}}}, k_{p_{3_{\min}}}] = [0.5823,\ 1.7,\ 0.97]$, while for the components of the derivative gain are as follows: $[k_{v_{1_{\min}}}, k_{v_{2_{\min}}},\ k_{v_{3_{\min}}}] = \left[2.4,\ 3.1,\ 1.55\right]$. On the other hand, the maximum values for the components of the proportional and derivative gains have been set as: $[k_{p_{1_{\max}}}, k_{p_{2_{\max}}}, k_{p_{3_{\max}}}] = [83.19, 138.65, 5.54]$ and $[k_{v_{1_{\max}}}, k_{v_{2_{\max}}}, k_{v_{3_{\max}}}] = [28.4, 32.3, 3.1]$.

The gains for the three evaluated control schemes $\boldsymbol{\tau}_{\mathrm{PD}}$, $\boldsymbol{\tau}_{\mathrm{atanh}}$ and $\boldsymbol{\tau}_{\mathrm{asinh}}$, must prevent saturation of actuators, which deteriorates the control system performance and leads to thermal and mechanical problems. Thus, we use the next fitness functions to obtain

Table 2. Tuning optimized by PSO algorithm for proportional and derivative gains.

Control scheme	Proportional gain	Derivative gain
$\boldsymbol{\tau}_{\text{PD}}$	$K_p = \text{diag}\{40.107,\ 50.0383,\ 5.093\}$ Nm/rad	$K_v = \text{diag}\{22.46, 31.5, 2.87\}$ Nm sec/rad
$\boldsymbol{\tau}_{asinh}$	$K_p = \text{diag}\{37.6027,\ 62.8375,\ 5.4352\}$ Nm	$K_v = \text{diag}\{13.2,\ 11.5,\ 2.64\}$ Nm
$\boldsymbol{\tau}_{\text{atanh}}$	$K_p = \text{diag}\{40.0262,\ 67.5914,\ 3.7289\}$ Nm	$K_v = \text{diag}\{25.612,\ 29.84,\ 3.62\}$ Nm

a transient response with few oscillations and vibrations as minimum as possible, better performance with accepted overshoot, rising time and settling time.

$$f_{k_{pi}}^{j+1}(\tilde{\boldsymbol{q}}_j(t)) = \frac{1}{T_{\text{exp}}}\sigma_{kp}\sum_{t=0}^{T_{\text{exp}}}\|\tilde{\boldsymbol{q}}_j(t)\|^2 \tag{18a}$$

$$f_{k_{vi}}^{j+1}(\dot{\boldsymbol{q}}_j(t)) = \frac{1}{T_{\text{exp}}}\sigma_{kv}\sum_{t=0}^{T_{\text{exp}}}[1 - 0.01e^{(-0.01\cosh(\dot{\boldsymbol{q}}_j(t)))}]^2 \tag{18b}$$

where $f_{k_{pi}}^{j+1}$ and $f_{k_{vi}}^{j+1}$ define the fitness values of the ith particle for the proportional and derivative gains related to mean error squared (MSE) criteria, respectively. $T_{\text{exp}} = 5$ s is the experimental time. The objective function is to determine the best $\boldsymbol{x}_i^{\text{best}}$ and best $\boldsymbol{x}_{gd}^{\text{best}}$ from (17a)–(17b).

The PSO algorithm uses the particle population size with $n_p = 25$, with $j = 15$ iterations. The update equations (17a) and (17b) are implemented in language C to find the optimal values within a 6-dimensional search space for the gains K_p and K_v. Each particle makes use of the previous position and current velocity information, while adjusting its own position to the best position in the swarm. However, several trials were required to ensure fast transient response, no oscillations, a minimum overshoot and smaller steady-state error, and keeping the actuators within their torque capabilities. According to the optimal fitness values of the particle that correspond to proportional and derivative gains, the optimized gains for each evaluated control $\boldsymbol{\tau}_{\text{PD}}$, $\boldsymbol{\tau}_{\text{atanh}}$ and $\boldsymbol{\tau}_{\text{asinh}}$ are selected by the position $\boldsymbol{x}_{gd}^{\text{best}}$ as shown in Table 2.

6.2. Experimental results of the PD control

Figure 3 shows the position errors of the control PD corresponding to three joints of the control $\boldsymbol{\tau}_{\text{PD}}$. Observe that after a smooth transient response, all the components tend asymptotically to a small neighborhood of equilibrium point. The transient response of position errors present small oscillations. A minimum overshoot is less than 0.02% with respect to the set-point q_{di}. Furthermore, the robot's response achieves stationary-state time shorter than 0.6 s. The position errors in steady-state (at $t = 0.6$ s) are $[\tilde{q}_1(t),\ \tilde{q}_2(t),\ \tilde{q}_3(t)]^{\text{T}} = [0.127,\ 0.233,\ 0.357]^{\text{T}}$ degrees. Therefore, the Euclidean norm at this time is $\|\tilde{\boldsymbol{q}}(0.6)\| = 0.4448$ degrees. A typical feature of PD control is that it presents an offset in stationary state, that is,

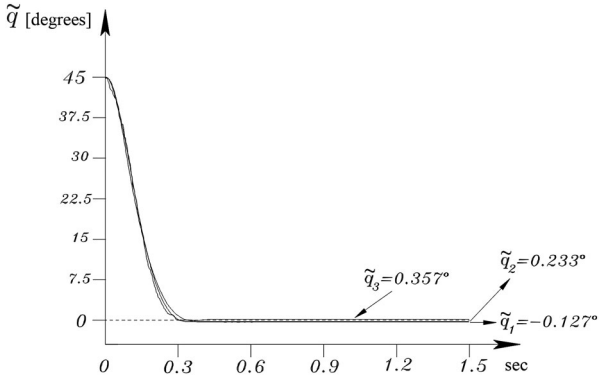

Figure 3. Position errors $\tilde{\boldsymbol{q}}(t)$ of the PD control.

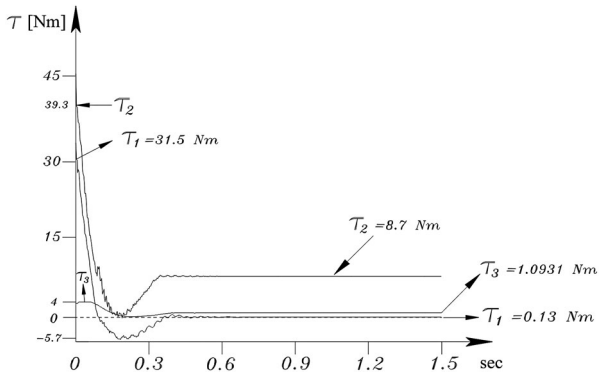

Figure 4. Applied torques of the PD control.

holds nonzero larger position errors due to the presence of static friction at the servomotors.

Figure 4 shows the applied control torques $\boldsymbol{\tau}_{\text{PD}}$ for each joint. Some oscillations in the transitory-state are observed in the applied torques. These oscillations are the effect of the derivative control action through damping injection to avoid over impulses and peaks in the position error signals. From experimental results, all torque signals clearly evolve inside the prescribed limits in Table 1.

6.3. Experimental results of the proposed control $\boldsymbol{\tau}_{\text{asinh}}$

The experimental results corresponding to the position errors of the proposed control asinh $\boldsymbol{\tau}_{\text{asinh}}$ are shown in Figure 5. All position errors converge to zero. A closer look reveals that at time $t = 0.8$ s, the steady-state is reached, that is, 0.2 s longer than in the case of the PD control $\boldsymbol{\tau}_{\text{PD}}$. However, control response $\boldsymbol{\tau}_{\text{asinh}}$ has better settling-time/overshoot. In other words, neither peak values nor overshoot are

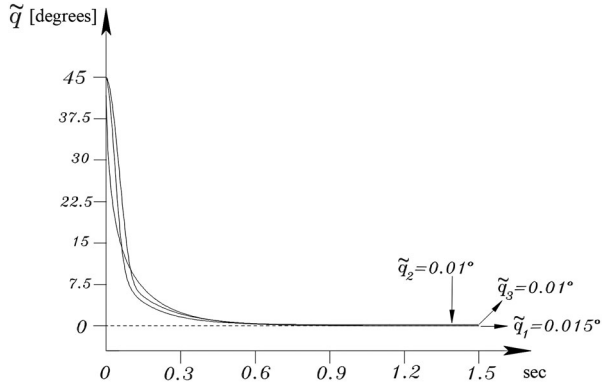

Figure 5. Position errors $\tilde{\boldsymbol{q}}(t)$ of the control $\boldsymbol{\tau}_{\text{asinh}}$.

presented. Then, the transient response is improved with respect to that of the PD control. This is due to the damping injection effect of the hyperbolic-type derivative control action $-K_v\,\text{asinh}(\dot{\boldsymbol{q}})$. Hence, the vector of position errors $\tilde{\boldsymbol{q}}(t)$ reduces its magnitude, without over-impulses, neither oscillations, nor vibrations. Because of the properties of the equilibrium point attractor, the vector of position errors converges asymptotically towards zero. The position errors in steady-state at $t = 0.8$ s for $\boldsymbol{\tau}_{\text{asinh}}$ are $[\tilde{q}_1(t),\ \tilde{q}_2(t),\ \tilde{q}_3(t)]^{\text{T}} = [0.01,\ 0.01,\ 0.015]^{\text{T}}$ degrees. Thus, the steady-state Euclidean norm is $\|\tilde{\boldsymbol{q}}(0.8)\| = 0.0206$ degrees. The PD control performance is improved by 59.798% through $\boldsymbol{\tau}_{\text{asinh}}$. Thus, the performance of the proposed control scheme $\boldsymbol{\tau}_{\text{asinh}}$ is much better than the control $\boldsymbol{\tau}_{\text{PD}}$.

Figure 6 shows the applied torque of the algorithm $\boldsymbol{\tau}_{\text{asinh}}$ to the robot's joints. It can be observed that the applied torques remain within the saturation limits. Observe a large excursion in each torque signal during the transitory phase. This is due to the derivative control action with hyperbolic structure. Its damping injection produces an over-damped type output (with behavior similar to a nonlinear damper that dissipates the motion generated by the velocity). The hyperbolic term that depends on the position error acts like a nonlinear spring. The control scheme $\boldsymbol{\tau}_{\text{asinh}}$ has the quality to drive the position error to zero, and obtains dissipation energy from the derivative term to achieve a response without overshoot, neither peaks. The control $\boldsymbol{\tau}_{\text{asinh}}$ increases its applied torque as high as it is required as shown in Figure 6, holding the actuator torque constraints. The transient response of the robot manipulator is good without excessive oscillations and the vector of position errors $\tilde{\boldsymbol{q}}(t)$ reaches smaller values in steady-state while, the servomotors are capable of holding the robot manipulator at rest for any desired joint positions vector $\boldsymbol{q}_d$. However, it should be mentioned that the torque signals present chattering, because the hyperbolic asinh function is implemented through the natural logarithm function: $\text{asinh}(\tilde{q}_i) = \ln(\tilde{q}_i + \sqrt{\tilde{q}_i^2 + 1})$, for $i = 1,\ 2,\ 3$, which presents numerical problems and overflow.

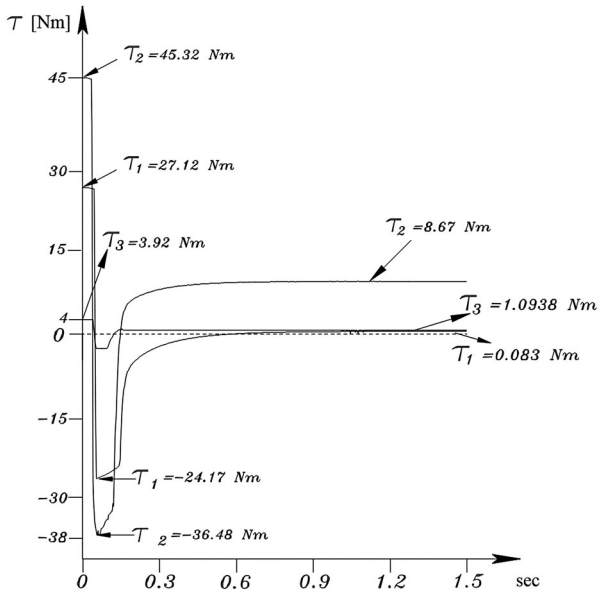

Figure 6. Applied torques of the asinh control.

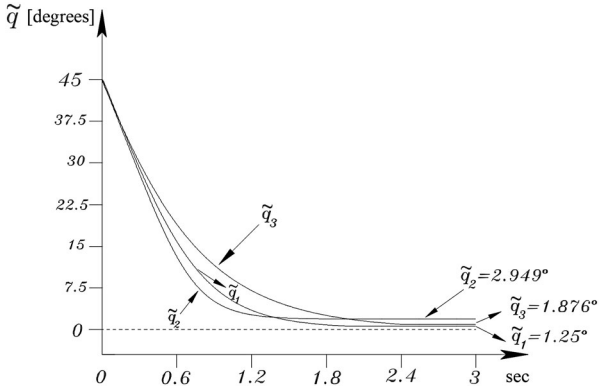

Figure 7. Position errors of the atanh control.

6.4. *Experimental results corresponding to the atanh control*

The experimental position errors for the control $\boldsymbol{\tau}_{\text{atanh}}$ are shown in Figure 7. The transient phase is very slow compared with the PD and asinh algorithms. In fact, the error signals take 2.6 s to reach the steady-state. In addition, the magnitudes of position errors are very large, which means that its performance is poor. For example, the error signals at $t = 2.6$ s are $[\tilde{q}_1(t),\ \tilde{q}_2(t),\ \tilde{q}_3(t)]^{\text{T}} = [1.876,\ 1.876,\ 2.949]^{\text{T}}$ degrees. Then, steady-state Euclidean norm is $\|\tilde{\boldsymbol{q}}(2.6)\| = 3.9668$ degrees, which is not competitive with any of the PD and asinh control schemes.

It is worth mentioning that the tuning process in the proportional and derivative control gains for $\boldsymbol{\tau}_{\text{atanh}}$ was very complicated due to the restrictions on $\tilde{\boldsymbol{q}}$. An overshoot in the response of the robot can cause that the atanh function returns imaginary values. It is not easy to obtain a competitive response with previous control schemes. Figure 8 illustrates the profile of the applied torques of the control scheme $\boldsymbol{\tau}_{\text{atanh}}$. Note that the torque response is fast. However, it logarithmically

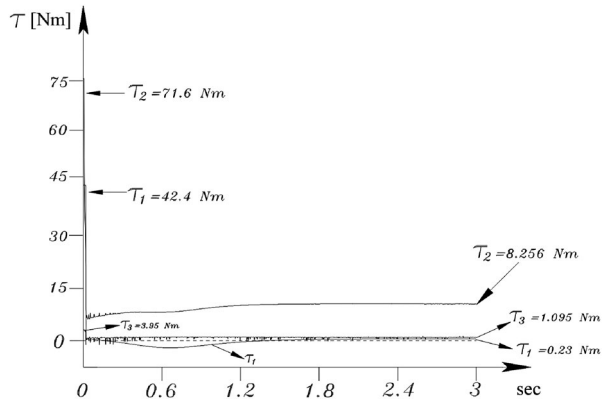

Figure 8. Applied torques of the atanh control.

decays, until it reaches a very small negative value. The torque signals have values below the static friction of the robot's servomotors, keeping the response in steady-state due to the gravitational torque with enormous magnitudes in $\tilde{\boldsymbol{q}}$.

6.5. Performance index

The performance of evaluated control schemes is measured to obtain faster transient and steady state response. Both requirements must be satisfied simultaneously. The control objective is achieved avoiding input saturation in all experiments. To measure this control objective, we use the root mean square of the norm $\mathcal{L}_2[\tilde{\boldsymbol{q}}(t)]$, which is an objective numerical measure for the position error $\tilde{\boldsymbol{q}}(t)$. It is given by [30]:

$$\mathcal{L}_2[\tilde{\boldsymbol{q}}(t)] = \sqrt{\frac{1}{T_{\text{exp}}}\int_0^T \|\tilde{\boldsymbol{q}}(\sigma)\|^2 \, \mathrm{d}\sigma} \qquad (19)$$

where $T_{\text{exp}} \in \mathbb{R}_+$ represents the experimental time (in our experiments, $T_{\text{exp}} = 5$ s). The smaller $\mathcal{L}_2[\tilde{\boldsymbol{q}}(t)]$ means smaller position error $\tilde{\boldsymbol{q}}(t)$ and it is the best evaluated controller performance. The control algorithm $\boldsymbol{\tau}_{\text{PD}}$ has a $\mathcal{L}_2[\tilde{\boldsymbol{q}}(t)] = 10.728$ degrees. The proposed control $\boldsymbol{\tau}_{\text{asinh}}$, $\mathcal{L}_2[\tilde{\boldsymbol{q}}(t)] = 6.735$ degrees, and for the scheme $\boldsymbol{\tau}_{\text{atanh}}$ with a $\mathcal{L}_2[\tilde{\boldsymbol{q}}(t)] = 19.59$ degrees. The performance of the PD control scheme is improved by 64% through the proposed control $\boldsymbol{\tau}_{\text{asinh}}$. With respect to the atanh control performance $\boldsymbol{\tau}_{\text{atanh}}$, it is roughly improved 290.87% by $\boldsymbol{\tau}_{\text{sinh}}$.

Another experimental test is carried out for 100 s with the generation of 20 random set-points $\boldsymbol{q}_d$ for the evaluated control schemes with the same tuning of gains. However, due to space limitations, we only present the corresponding numerical results of the average Euclidean-norm and the norm $\mathcal{L}_2[\tilde{\boldsymbol{q}}(t)]$ corresponding to each evaluated control. The random sequence is obtained by using each 5 s an uniformly distribution random set-points between 0 and $\frac{\pi}{4}$ rad: $q_{di} = \frac{\pi}{4}\,\text{rand}(\cdot)$, where rand$(\cdot)$ is the random function, which returns a random numbers in the interval (0, 1); q_{di} is ith set-point for $i = 1, 2, 3$ corresponding to the base, elbow and shoulder joints, respectively. In this experimental phase, the average of the error norms for comparison is: $\|\tilde{\boldsymbol{q}}(t)\|_{\text{PD}} = 0.63$ degrees, $\|\tilde{\boldsymbol{q}}(t)\|_{\text{asinh}} = 0.031$ degrees and $\|\tilde{\boldsymbol{q}}(t)\|_{\text{atanh}} = 4.93$ degrees corresponding to $\boldsymbol{\tau}_{\text{PD}}$, $\boldsymbol{\tau}_{\text{asinh}}$ and $\boldsymbol{\tau}_{\text{atanh}}$, respectively. On the other hand, the average of the norms $\mathcal{L}_2[\tilde{\boldsymbol{q}}(t)]$ for each evaluated scheme is: $\boldsymbol{\tau}_{\text{PD}}$ has a $\mathcal{L}_2[\tilde{\boldsymbol{q}}(t)] = 11.55$ degrees, for $\boldsymbol{\tau}_{\text{asinh}}$, $\mathcal{L}_2[\tilde{\boldsymbol{q}}(t)] = 7.14$ degrees, and for $\boldsymbol{\tau}_{\text{atanh}}$ with a $\mathcal{L}_2[\tilde{\boldsymbol{q}}(t)] = 21.42$ degrees. Note that a similar performance ratio is maintained for the above case $\boldsymbol{q}_d = [\frac{\pi}{4}, \frac{\pi}{4}, \frac{\pi}{4}]^{\text{T}}$ rad. In general, $\boldsymbol{\tau}_{\text{asinh}}$ shows better performance (smaller $\mathcal{L}_2[\tilde{\boldsymbol{q}}(t)]$) than the PD and atanh algorithms. Therefore, the usefulness of proposed methodology is shown experimentally and it represents an attractive solution of nonlinear control for industrial applications and process automation.

7. Future research

The proposed control scheme $\boldsymbol{\tau}_{\text{asinh}}$ (6) keeps the constant gains K_p and K_v. A further research is to analyze the global asymptotic stability for the control version with variable gains $K_p(\tilde{\boldsymbol{q}})$ and $K_v(\dot{\boldsymbol{q}})$, and to propose an automatic tuning-procedure for these gains and to study the performance of an experimental robot.

8. Conclusions

In this paper, we have presented an new control scheme with asinh-type structure to solve the position control problem of robot manipulators in joint space. The proposed scheme is supported by a rigorous global asymptotic stability analysis in the sense of Lyapunov. We have designed a strict Lyapunov function to establish conditions for ensuring global regulation.

The performance of evaluated control schemes is measured to obtain good transient and better steady state response. Based on the real-time experimental results on a three degree-of-freedom direct-drive robot manipulator, the performance of the proposed control scheme has been compared with the PD and atanh control algorithms. The tuning of the control gains is obtained by a PSO algorithm avoiding saturation in the applied control signals to the robot's servomotors. It is corroborated that the analytical result and the asinh control structure is more efficient than the other evaluated schemes

The proposed control has good transient response and small steady-state position errors. Its mathematical properties allow leading the position error to zero. The control objective is achieved avoiding input saturation in the experiments.

The effectiveness of the proposed asinh control have been verified, because it shows great advantages over its counterparts. It permits the implementation of potential applications. Our contribution helps, if modestly,

to the development of a new control algorithm which effectively exploits its properties like a nonlinear spring to restore the position error to equilibrium point and hyperbolic energy dissipation similar to a nonlinear damper to obtain the transient-state response without overshoots.

Acknowledgements

The authors would like to thank the Benemerita Universidad Autonoma de Puebla, for its financial support with the project VIEP-100048866-2019 (Control de posición con ganancias variables de robots manipuladores), which partially supported this work.

Disclosure statement

No potential conflict of interest was reported by the author(s).

Funding

The authors would like to thank the Benemerita Universidad Autonoma de Puebla, for its financial support with the project VIEP-100048866-2019 (Control de posición con ganancias variables de robots manipuladores), which partially supported this work.

ORCID

Fernando Reyes-Cortes http://orcid.org/0000-0001-5200-7632

References

[1] Siciliano B, Kathib O. Handbook[Q2] of robotics. 2nd ed. Berlin Heidelberg: Springer; 2016.
[2] Kelly R, Santibañez V, Loria A. Control of robot manipulators in joint space. London: Springer; 2005.
[3] Takegaki M, Arimoto S. A new feedback method for dynamic control of manipulators. ASME J. Dyn. Syst. Meas. Control. 1981;103:119–125.
[4] Zavala A, Mendoza M, Santibañez V, et al. Output-feedback proportional-integral-derivative-type control with multiple saturating structure for the global stabilization of robot manipulators with bounded inputs. Int J Adv Robot Syst. 2016;6:1–12.
[5] Santibañez V, Kelly R, Llama MA. A novel global asymptotic stable set-point fuzzy controller with bounded torques for robot manipulators. IEEE Trans Fuzzy Syst. 2005;13(3):362–372.
[6] Ramirez JA, Santibañez V, Campa R. Stability of robot manipulators under saturated PID compensation. IEEE Trans Control Syst Technol. 2008;16(6):1333–1341.
[7] Sun D, Hu S, Shao X, et al. Global stability of a saturated nonlinear PID controller for robot manipulators. IEEE Trans Control Syst Technol. 2009;17(4):892–899.
[8] Su Y, Muller PC, Zheng C. Global asymptotic saturated PID control for robot manipulators. IEEE Trans Control Syst Technol. 2010;18(6):1280–1288.
[9] Yarza A, Santibañez V, Moreno J. Global asymptotic stability of the classical PID controller by considering saturation effects in industrial robots. Int J Adv Robot Syst. 2011;8(4):34–42.
[10] Fischer N, Dani A, Sharma N, et al. Saturated control of an uncertain nonlinear system with input delay. Automatica. 2013;49:1741–1747.
[11] Caverly RJ, Zlotink DE, Bridgeman LJ, et al. Saturated proportional derivative control of a single-link flexible-joint manipulator. Robot Comput Integr Manuf. 2014;30:658–666.
[12] Hu J, Zhang H. Globally asymptotically stable saturated PID controllers for a double integrator with constant disturbance. Int J Robust Nonlinear Control. 2014;24:1488–1504.
[13] Mendoza M, Zavala A, Santibañez V, et al. Output-feedback proportional-integral-derivative-type control with simple tuning for the global regulation of robot manipulators with inputs constraints. IET Control Theory Appl. 2017;9:2097–2106.
[14] Salinas A, Moreno J, Kelly R. A family of nonlinear PID-like regulators for a class of torque-driven robot manipulators with torque-constrained actuators. Adv Mech Eng. 2016;8(2):1–14.
[15] Romero JG, Ortega R, Donaire A. Energy shaping of mechanical systems via PID control and extensions to constant speed tracking. IEEE Trans Automat Contr. 2016;161(11):3551–3556.
[16] Wang H, Su Y, Zhang L. Global output feedback position regulation of friction robot manipulators. Proc IMechE Part I: J Syst Control Eng. 2017;231:230–241.
[17] Adhikary N, Mahanta C. Inverse dynamics based robust control method for position commanded servo actuators in robot manipulators. Control Eng Pract. 2017;6:146–155.
[18] Su Y, Zheng C. PID control for global finite-time regulation of robotic manipulators. Int J Syst Sci. 2017;48(3):547–558.
[19] Liu Z, Liu J. Boundary control of a flexible robotic manipulator with out constraints. Asian J Control. 2017;19(1):332–345.
[20] Qahtani HM, Mohammed A, Sunar M. Dynamics and control of robotic arm having four links. Arab J Sci Eng. 2017;42:1841–1852.
[21] Hernandez VM, Orrante J. Global PID control of robot manipulators equipped with PMSMS. Asian J Control. 2018;20(1):236–249.
[22] Galvan V, Hernandez VM, Orrante J. PID position regulation in one-degree-of-freedom Euler-Lagrange systems actuated by a PMSM. Int J Control. 2018;91(2):285–296.
[23] del Petre A. Joint position and velocity bounds in discrete-time acceleration/torque control of robot manipulators. IEEE Robot Autom Lett. 2018;3(1):281–288.
[24] Izadbakhsh A, Kheirkhahan P. Nonlinear PD control of electrical flexible joint robots-theory and experimental verification. 2018 IEEE International Conference on Industrial Technology (ICIT); 2018 Feb 19–22; Lyon, France. p. 250–255.
[25] Kelly R, Santibañez V. Global regulation of elastic joint robots based on energy shaping. IEEE Trans Automat Contr. 1998;43(10):1451–1456.
[26] Santibañez V, Kelly R, Reyes F. A new set-point controller with bounded torques for robot manipulators. IEEE Trans Ind Electron. 1998;45(1):126–133.
[27] Reyes F, Cid J, Limon M, et al. Square root-type control for robot manipulators. Int J Adv Robot Syst. 2013;10(39):1–7.
[28] Reyes F, Chavez C, Gonzalez E. A family of hyperbolic-type explicit force regulators with active velocity damping for robot manipulators. J Robot. 2018;2018:1–15.
[29] Zhu L. New inequalities of Shafer-Fink type for arc hyperbolic sine. J Inequal Appl. 2008;2008:1–5.

[30] Chaudhary H, Panwar V, Prasad R, et al. Adaptive neural fuzzy hybrid force/position for an industrial robot manipulator. J Intell Manuf. 2016;27(6):1299–1308.
[31] Kennedy J, Eberhart RC. Particle swarm optimization. Proceedings of the IEEE International Conference on Neural Networks. Perth, WA, Australia. Vol. 4; 1995. p. 1942–1948.
[32] Shi Y, Eberhart RC. A modified particle swarm optimizer. IEEE International Conference on Evolutionary Computation. Anchorage, AK, USA, 1998. p. 69–73.
[33] Shi Y, Eberhart RC. Particle swarm optimization: developments, applications and resources. IEEE Proceedings of the 2001 Congress on Evolutionary Computation. Seoul, South Korea. Vol. 1; May 2001. p. 81–86.
[34] Clerc M, Kennedy J. The particle swarm–explosion, stability, and convergence in multidimensional complex space. IEEE Trans Evol Comput. Feb 2002;6(1):58–73.